SCIENCE CHINA
Physics, Mechanics & Astronomy

•Article•

October 2020 Vol. 63 No. 10: 104612
https://doi.org/10.1007/s11433-020-1543-8

Theoretical study of the effects of alloying elements on Cu nanotwins

Jun Hui, Wenguan Liu*, and Biao Wang*

Sino-French Institute of Nuclear Engineering and Technology, Sun Yat-Sen University, Zhuhai 519082, China

Received January 11, 2020; accepted March 10, 2020; published online April 23, 2020

Nanotwins form in many metallic materials to improve their strength and toughness. In this study, we thoroughly studied the alloying effects of 10 common metal and nonmetal elements on Cu nanotwins by density functional theory (DFT). We calculated the segregation energies to determine if Cu nanotwins attract both the metal and nonmetal alloying elements; these segregation energies were then decomposed to mechanical and chemical components. The Cu-Sn bonds are different from other metal alloying elements, and the strong bond between Cu and the nonmetal element results in the negative values of the chemical contribution. Furthermore, the temperature and concentration have different effects on the nanotwin formation energy of the metal and nonmetal alloying elements. As determined by the Generalized Stacking Fault Energy, Al and nonmetals can inhibit the migration of Cu nanotwin boundary, and the effects of Li, Mg, and Sn are opposite. Our theoretical study serves as the foundation for the engineering nanotwin structures through alloying elements, the elements that may lead to new alloy compositions and thermomechanical processes, and are important complements to the experimental research.

nanotwin, alloying element, density functional theory, segregation energy, nanotwin formation energy, generalized stacking fault energy

PACS number(s): 68.35.Dv, 61.72.Mm, 61.72.Nn, 71.15.Mb

Citation: J. Hui, W. Liu, and B. Wang, Theoretical study of the effects of alloying elements on Cu nanotwins, Sci. China-Phys. Mech. Astron. **63**, 104612 (2020), https://doi.org/10.1007/s11433-020-1543-8

1 Introduction

New microstructures often exhibit new macroscopic properties, thus triggering new application prospects. Introducing nanocrystalline structures into metals can lead to new mechanisms and electrical properties and this will broaden the range of their applications in engineering [1-5]. However, the strength-ductility trade-off has been a long-standing dilemma in materials science; for instance, some studies [6-10] have shown that the non-coherent high-energy grain boundary cannot continue strengthening the metal. To solve this problem, the high-energy disordered grain boundary should be replaced with other interfaces with a low mismatch —the coherent interface.

The introduction of nanotwins to Cu alloys has been widely studied because of the low stacking fault energy of Cu [11]. Lu et al. [12], in a scientific review, argued that the introduction of nanotwin is an effective way to improve metal strengthening and toughness. However, it is very difficult to introduce nanotwins into FCC metals (e.g., Cu). At room temperature, the twinning shear strain of FCC metal is the largest; thus, the formation energy of the FCC nanotwin has extreme instability, which calls for a high strain rate and cryogenic liquid nitrogen to form a nanotwin [13].

To address this problem, Zhao et al. [14-17] proposed

*Corresponding authors (Wenguan Liu, email: liuwg7@mail.sysu.edu.cn; Biao Wang, email: wangbiao@mail.sysu.edu.cn)

adjusting the stacking fault energy, known to be closely associated with the formation of nanotwin, through alloying elements in Cu alloys. They deemed this adjustment an effective way to control the microstructure of metals leading to the simultaneous improvement of strength and toughness. Lu et al. [12] reported that the lower nanotwin formation energies induced by Al in Cu alloys can lead to thinner twins via pulse electrodeposition, because the nanotwin formation energy is closely associated with twinning and other mechanisms [18-24]. In addition, Nie et al. [25] found that Zn and Gd have an obvious segregation tendency at twin boundary and exert a pinning effect on twins, in which annealing strengthens not weakens these alloys. Therefore, alloying elements have an important effect on the nucleation and growth of nanotwin, which should be further studied.

Experimentally, it is relatively difficult to detect the alloying atoms at the twin boundary. However, first-principles calculations can be used to study the physical mechanism on the atomic and electronic levels [26-30]; for instance, the alloying atoms at the twin boundary [31]. Until recently, most researchers have been focusing on pure twins without considering the effects of alloying elements [32-34]. As a result, the effects of alloying atoms on the nanotwins in Cu alloys have been addressed by first-principles calculations in this study.

Furthermore, to describe the dynamic nanotwin formation energies and boundary energy change process at an atomic scale, Vítek [35] proposed the concept of Generalized Stacking Fault Energy (GSFE), which is the free energy plane corresponding to the continuous state change process; it describes the atomic-level shear process on the slip plane. First-principles calculations can be used to calculate GSFE [36-38].

In this study, the mechanism of the effects of alloying atoms on Cu nanotwins was studied quantitatively and systematically by first-principles calculations. The studied alloying elements include common metal elements (i.e., Li, Mg, Al, Zn, and Sn) and nonmetal ones (i.e., C, N, O, P, and S) in Cu alloys. Our findings in this work provide a theoretical support for engineering nanotwin structures through alloying elements. This may lead to new alloy compositions and thermomechanical processes.

2 Calculational details

The FCC crystal is made of {111} faces, and ...*BCABCAB-CA*... units are sequentially stacked, and this stacking order can change from one layer to another; for instance, layer *B* moves to layer *C* and layer C moves to layer *A*. By analogy, the stacking order becomes…*BCABC**A**CBA*…, where *A*, *B,* and *C* are the atomic stacking layers in (111) atomic planes, and the underlined layers indicate the twin planes; here, ***A*** is called the nanotwin boundary.

Figure 1 shows the supercell used to calculate the segregation energy (SE). It is constructed as follows: $3e_1 \times 3e_2 \times me_3$, $e_1 = a/2$ [1 1 0], $e_2 = a/2$ [–1 1 0], $e_3 = a/2$ [1 –1 1]; m denotes the number of atomic layers in nanotwin supercell. The x-axis of the matrix is along the direction [–1 –1 2], the y-axis [1 1 1] direction, and the z-axis [1 –1 0] direction; here, the 4, 6, 8, and 10 layers of nanotwin (lnt) models are established. The total number of atoms in the five models are 36, 54, 72 and 90, respectively. The multilayer nanotwin is symmetrical with respect to the nanotwin plane; thus, nanotwin on either side can be selected as the research object. The nanotwin boundary is defined as 0 (denoted by $n = 0$) layer, and the nearest atomic plane to the nanotwin boundary is the $n = 1$ layer. Substitutional atoms (denoted by X, X_1 = Li, Mg, Al, Zn, and Sn) were added to the n layer, and interstitial atoms (X_2 = C, N, O, P, and S) were added to the interstitial positions of each layer. The nearest interstitial atoms to the nanotwin boundary are labeled as the 0 layer.

We only considered the substitutional atoms, discussed in sect. 3.4, when calculating GSFE in this study [36-38]. The supercell, shown in Figure 2(a), used to calculate GSFE is constructed as follows: $e_1 \times e_2 \times 3e_3$, $e_1 = a/2$ [–1 1 0], $e_2 = a/2$ [–1 –1 2], $e_3 = a/2$ [1 1 1]. This supercell contains 21 layers of the slip plane (excluding the vacuum layer), which are marked as L01-L21. In Figure 2(b), a single twin grain boundary is introduced into L10 layer, and a substitutional atom is doped in L11 layer, which is denoted as NTB1 configuration. In Figure 2(c), another single nanotwin boundary is introduced at L11 layer in NTB2 configuration. The evolution from NTB1 to NTB2 means the diffusion process of a single nanotwin boundary across a substitutional atom and the effect of the substitutional atom on the mobility of nanotwin can be measured effectively by diffusion barrier during the process.

We used the Vienna *ab initio* simulation package (VASP) [39,40] to calculate the electronic state within the density functional theory [41,42]. Electron-ion interactions were described by the projector-augmented plane-wave (PAW) [43] method. A generalized gradient approximation (GGA) [44-46] of the exchange-correlation energy was used. The total energy and Hellmann-Feynman forces were convergent within 10^{-6} eV and 10^{-2} eV/Å, respectively, with a cutoff energy of 400 eV. We then screened 10 common kinds of alloying elements in Cu after a large amount of calculation in the previous period. The number of valence electrons for pseudopotentials used are as follows: 11 for Cu ($3d^{10}$,$4s^1$), 3 for Al ($3s^2$,$3p^1$), 1 for Li ($2s^1$), 2 for Mg ($3s^2$), 5 for P ($3s^2$,$3p^3$), 6 for S ($3s^2$,$3p^4$), 4 for Sn ($5s^2$,$5p^2$), 12 for Zn ($3d^{10}$,$4s^2$), 4 for C ($2s^2$,$2p^2$), 5 for N ($2s^2$, $2p^3$) and 6 for O ($2s^2$, $2p^4$). The K-points of the four supercells in Figure 1 were 5×5×5 (4lnt), 5×5×4 (6lnt), 5×5×3 (8lnt) and 5×5×2 (10lnt) according to the dimensions of supercells, and the

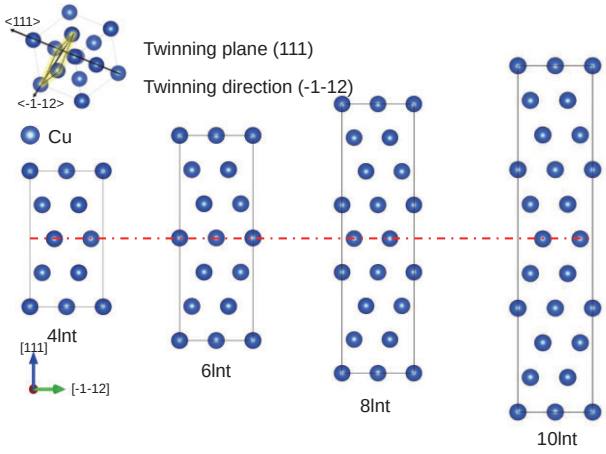

Figure 1 (Color online) Four kinds of nanotwin supercell models are shown. The red line represents the plane of nanotwin boundary.

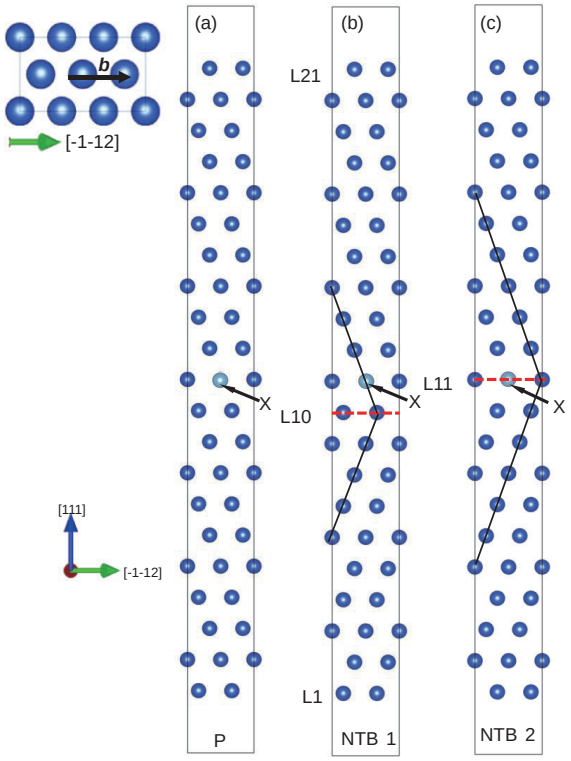

Figure 2 (Color online) (a) Perfect supercell of FCC Cu. (b) L10 is the nanotwin boundary in the Cu NTB1 supercell. X represents the substitutional atom. Atoms move in the direction of ***b***: The vector ***b*** = 1/6 [–1 –1 2] is one partial Shockley dislocation. (c) Based on the NTB1 supercell in (b), the atom layers above L11 slips 1/3 along ***b*** to form NTB2. The red line denotes the nanotwin plane.

corresponding K-points were changed into 15×9×2 for the supercell in Figure 2. In order to calculate the diffusion process of nanotwin, the supercells in Figure 2 should be longer than in Figure 1. Nanotwin formation energy was calculated based on the climbing-image nudged elastic band method (CNEB), and the three images were inserted into the beginning and the ending intervals [47].

3 Results and discussion

3.1 Segregation energy of alloying element in Cu nanotwin

First, the segregation energies (SEs) of alloying elements in the nanotwin supercells were investigated to identify the stable sites for alloying elements, which can determine the segregation tendency of alloying elements and reflect the relationship between the alloying elements and the nanotwin. According to refs. [48-50], the SE in Cu nanotwin supercell, E_{SE}, can be calculated as follows:

$$E_{SE} = \left[E(\mathrm{Cu}_{\mathrm{nanotwin}}X) - E(\mathrm{Cu}_{\mathrm{nanotwin}})\right] - \left[E(\mathrm{Cu}_{\mathrm{FCC}}X) - E(\mathrm{Cu}_{\mathrm{FCC}})\right], \quad (1)$$

where $E(\mathrm{Cu}_{\mathrm{nanotwin}})$ and $E(\mathrm{Cu}_{\mathrm{nanotwin}}X)$ are the calculated energies of the Cu nanotwin supercells without and with a solute X, respectively, and $E(\mathrm{Cu}_{\mathrm{FCC}})$ and $E(\mathrm{Cu}_{\mathrm{FCC}}X)$ are the calculated energies of the perfect FCC Cu supercells without and with a solute X, respectively. A positive value of E_{SE} means the mutual attraction between the alloying atom and nanotwin, and a negative suggests the mutual rejection between them. When SE < 0, the alloying atom can segregate easily to the nanotwin, and vice versa [48,49].

The crystal structure relationship of Cu $\{111\}\langle 1\,1\,-2\rangle$ twin used in this work is displayed in Figure 3(a), and the nanotwin supercells in Figures 1 and 3 were constructed according to these crystallographic parameters. Figures 3(a) and (b) display the atomic environments of substitutional and interstitial sites, respectively. Table 1 shows the calculated SEs of both substitutional elements (i.e., Li, Al, Mg, Zn and Sn) and interstitial elements (i.e., C, N, O, P, and S) at different atomic sites of the four types of the nanotwin supercells in Figure 1.

As shown by Table 1, the calculated SEs of the alloying elements increase linearly with the distance of alloying atoms from the nanotwin boundary in all the four kinds of nanotwins in Figure 1. For the cases of interstitial elements (i.e., C, N, O, P, and S), the calculated SEs in Table 1 are always negative for the sites at the nanotwin boundary; therefore, Cu nanotwin attracts alloying elements, especially interstitial nonmetal ones. However, in contrast with the results of 4lnt, 6lnt, 10lnt in Table 1, the SEs of substitutional metal elements in 6lnt supercell are negative, and this result is directly associated with the special structure of 6lnt that has the perfect stacking order *ABCCBA*.

As shown in Table 1, the attraction of alloying atoms to the nanotwin boundary decreases gradually as they are away from the nanotwin boundary. The alloying atoms are more stable when they are on or close to the nanotwin boundary. Kumar et al. [31] studied the twinning-associated boundaries in hexagonal metals with first-principles calculations and found that the solubility of solid-soluble atoms at the co-

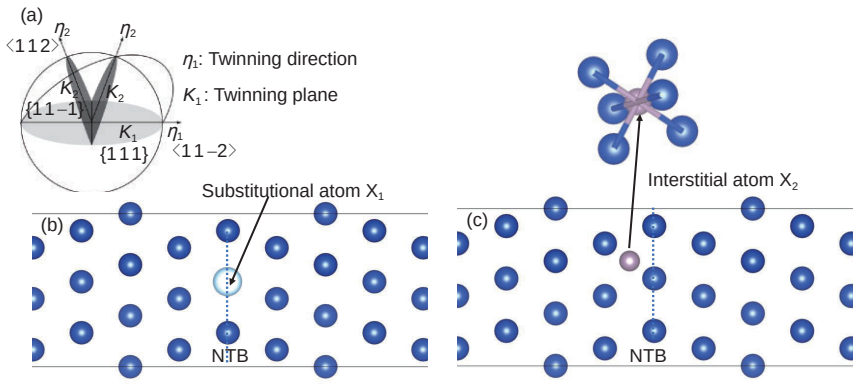

Figure 3 (Color online) (a) The crystal structure relationship of Cu $\{111\}\langle 1\,1\,-2\rangle$ twin. (b) The substitutional site in the nanotwin plane, which is denoted by the white ball. (c) The octahedral interstitial site nearest to the nanotwin plane, which is represented by the grey ball.

Table 1 It shows the calculated SEs (meV) of 10 kinds of metal and nonmetal elements in different atomic sites of Cu nanotwin supercell. For metal elements, "0" indicates the substitutional site that is at the twin plane (i.e., the site of the white ball in Figure 3(b)), and "1" denotes the site that is nearest to the twin plane, and so on. For nonmetal elements, "0" indicates the octahedral interstitial site that is nearest to the twin plane (i.e., the site of the grey ball in Figure 3(c)), and "1" denotes the site that is secondly nearest to the twin plane, and so on

Atom	4lnt		6lnt		8lnt			10lnt		
	0	1	0	1	0	1	2	0	1	2
Li	–24.6	29.6	–10.3	4.1	150.6	159.7	165.9	45.7	55.9	58.3
Mg	128.0	129.6	–57.4	–36.6	192.9	200.9	210.8	128.2	140.9	148.5
Al	36.2	74.3	–49.4	–38.1	163.3	168.7	170.9	140.7	149.9	160.5
Zn	82.5	84.5	–49.4	–39.3	193.0	200.9	210.8	122.4	129.3	135.6
Sn	39.9	78.2	–99.4	–81.6	126.8	127.8	165.5	96.4	103.6	129.8
C	–169.7	–	–184.2	–117.0	–18.9	58.5	–	–69.0	2.3	21.8
N	–245.0	–	–198.5	–101.6	–49.9	64.0	–	–146.8	–45.3	26.9
O	–225.5	–	–188.3	–69.3	–46.1	87.2	–	–157.1	–39.6	–22.8
P	–221.4	–	–157.5	–84.1	34.4	129.9	–	–24.8	81.5	106.9
S	–250.9	–	–160.1	–52.2	–3.4	135.8	–	–93.7	36.3	65.1

herent twin boundary is greater than in bulk, which is in good agreement with the case of Cu nanotwin in this work. Nie et al. [25] studied the annealing hardening of Mg by HRTEM and first-principles calculations, and showed that the twin boundary can accommodate the solid solution atoms Zn, which is also consist with our results.

3.2 Atomic and electronic structures around alloying element in nanotwin

It is crucial to understand the structure and chemistry of nanotwin boundaries influenced by the alloying elements. To explore further the physical origins of the SE, we decomposed the SE into two components: (i) the mechanical contribution (E_{me}) (resulting from the mismatch of atomic size) and (ii) the chemical contribution (E_{ce}) (closely related with charge distributions). Thus, the SE can be decomposed as follows:

$$E_{SE} = E_{me} + E_{ce}. \tag{2}$$

The mechanical contribution, E_{me}, can be calculated as:

$$E_{me} = \left[E(\mathrm{Cu}_{\mathrm{nanotwin}}X) - E(\mathrm{Cu}_{\mathrm{nanotwin}}XF)\right] - \left[E(\mathrm{Cu}_{\mathrm{FCC}}X) - E(\mathrm{Cu}_{\mathrm{FCC}}XF)\right], \tag{3}$$

where $E(\mathrm{Cu}_{\mathrm{nanotwin}}XF)$ (or $E(\mathrm{Cu}_{\mathrm{FCC}}XF)$) is the calculated energy of the pure Cu nanotwin supercell (or the pure FCC Cu supercell) in which a Cu atom is replaced by a substitutional alloying atom X or an interstitial atom X is inserted in an octahedral interstitial site, but all the atomic coordinates are kept unchanged. Accordingly, the chemical component, E_{ce}, can be calculated as follows:

$$E_{ce} = \left[E(\mathrm{Cu}_{\mathrm{nanotwin}}XF) - E(\mathrm{Cu}_{\mathrm{nanotwin}})\right] - \left[E(\mathrm{Cu}_{\mathrm{FCC}}XF) - E(\mathrm{Cu}_{\mathrm{FCC}})\right]. \tag{4}$$

The calculated E_{me} and E_{ce} of the alloying elements in 4lnt are shown in Figure 4. For most metal atoms (except Sn), the chemical component is bigger than the mechanical one, but the case of Sn is opposite. On the other hand, for all the calculated nonmetal atoms in Figure 4, the chemical component contributes the major part of the SE and plays a

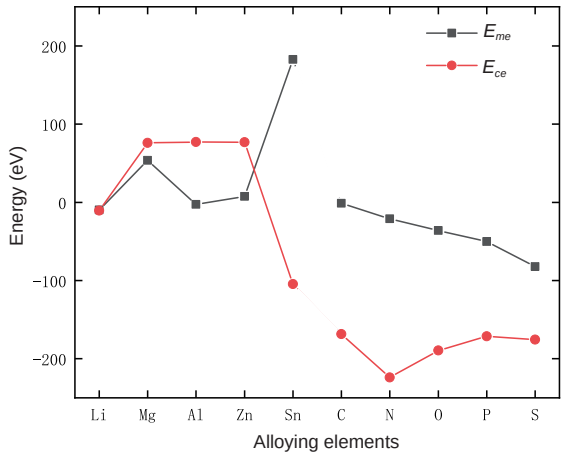

Figure 4 (Color online) The calculated chemical (E_{ce}) and mechanical components (E_{me}) of the SEs in 4lnt supercell where the metal atom occupies a substitutional site in the nanotwin plane or the nonmetal atom occupies an interstitial site nearest to the nanotwin plane.

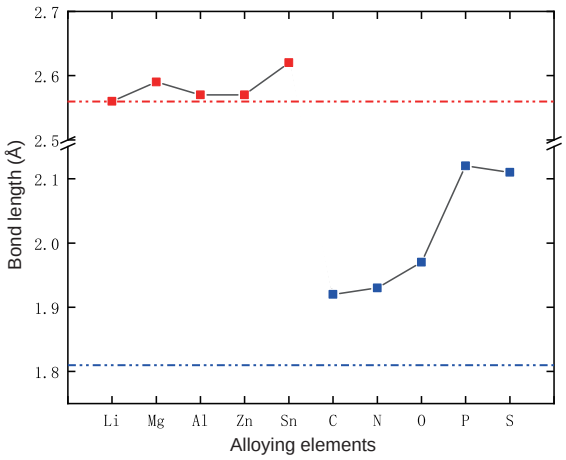

Figure 5 (Color online) The calculated shortest Cu-X bond length in 4lnt supercell, and X represents the substitutional metal element or interstitial nonmetal one. The red dotted line denotes the length of the corresponding Cu-Cu bond with the value of 2.56 Å in pure Cu 4lnt supercell, and the blue dotted one refers to the distance between the corresponding Cu atom and the center of octahedral interstitial site with the value of 1.81 Å in pure Cu 4lnt supercell.

dominant role, and the mechanical one only reduces its value.

It can be seen in Figure 4 that the differences between mechanical and chemical components for most substitutional metal elements (except Sn) are much smaller than those for nonmetal elements. Moreover, the chemical component contributes the major part of the SE.

Local expansion or shrinkage can be induced by alloying atoms at the substitutional or interstitial site in the nanotwin supercells, which will lead to changes in the mechanical component, E_{me}. The shortest distance between Cu and the alloying atom can be used to describe the misfit volume of the alloying atom. The shortest Cu-alloying atom bond lengths in 4lnt supercell were calculated and shown in Figure 5. Figure 5 shows that almost all the calculated metal elements can induce local expansion, and the change trend for these metal elements is in good agreement with that of the mechanical components in Figure 4. Furthermore, the insertion of the nonmetal elements into the octahedral interstitial site can also induce local expansion, because the interstitial site is not big enough to accommodate the nonmetal elements.

As stated above, the chemical contribution (E_{ce}) is closely related with the chemical bonding and the charge distribution upon addition of solute atoms on the nanotwin. The calculated charge densities for the substitutional metal atoms are displayed in Figure 6. The charge accumulation between Cu and Sn is denser than that between Cu and the other substitutional atom. Thus, the Cu-Sn bonds are stronger and beneficial for Sn to segregate into the nanotwin boundary, which is in good agreement with the negative value of the chemical component of Sn in Figure 4.

The calculated charge densities around the interstitial nonmetal atoms are shown in Figure 7. The bonds between Cu and the nonmetal elements are different from the typical metal Cu-Cu bonds (and the bonds between Cu and the metal alloying elements) and also stronger. This can be judged from the much denser charge density between them. These strong bonds are beneficial to the segregation of the nonmetal elements by resulting in the negative values of chemical contributions in Figure 4.

3.3 Nanotwin formation energy

The nanotwin formation energy is directly associated with the processes of twinning and detwinning, and it denotes the energy difference between the nanotwin configuration and the perfect structure per area. The larger the formation energy, the more difficult it is to form a twin configuration [49].

The pure Cu nanotwin formation energy can be calculated as follows:

$$\gamma_0 = \frac{E(\mathrm{Cu_{nanotwin}}) - E(\mathrm{Cu_{FCC}})}{2A}, \tag{5}$$

where A is the area of (111) plane of the nanotwin supercell in Figure 1, $E(\mathrm{Cu_{nanotwin}})$ and $E(\mathrm{Cu_{FCC}})$ are the total energies of Cu nanotwin supercell and Cu FCC structure with the same number of Cu atoms, respectively.

When the alloying element X is introduced into the nanotwin, the nanotwin formation energy, γ_{0X}, is calculated as follows:

$$\gamma_{0X} = \frac{E(\mathrm{Cu_{nanotwin}}X) - E(\mathrm{Cu_{FCC}}X)}{A} - \gamma_0. \tag{6}$$

As shown in Figure 8, the formation energy of different Cu nanotwins is distributed between 20 and 40 mJ/m^2. Compared with the case of pure Cu in Figure 8, the metal substitutional atoms increase the nanotwin formation energy,

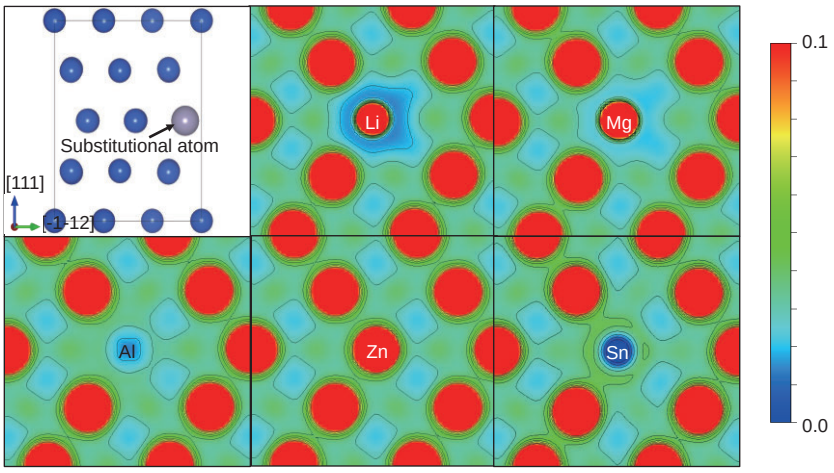

Figure 6 (Color online) Calculated charge density (e/Bohr^3) in the 4lnt supercell for the substitutional metal atoms (i.e., Li, Mg, Al, Zn, and Sn) at the plane of nanotwin boundary.

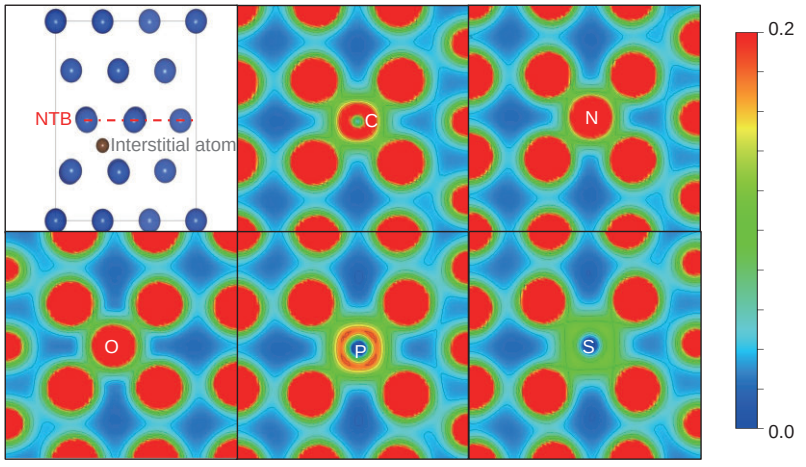

Figure 7 (Color online) Calculated charge density (e/Bohr^3) in the 4lnt supercell. The interstitial (i.e., C, N, O, P, and S) nonmetal atoms are in the center and surrounded by Cu atoms. The position of the nonmetal element is shown in the first graph.

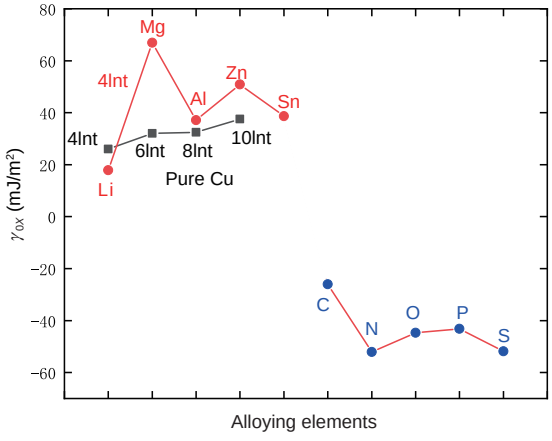

Figure 8 (Color online) The nanotwin formation energy of pure and doped Cu nanotwin systems. The black line indicates γ_0 in pure Cu 4lnt, 6lnt, 8lnt and 10lnt. The values of γ_{0x} for the alloying elements were calculated in 4lnt with the metal elements in X_1 site or the nonmetal elements in X_2 site in Figure 3.

and nonmetal interstitial atoms reduce it. Thus, Li, Mg, Al, Sn and Zn atoms hinder the formation of nanotwin and promote the detwinning process, and the effects of C, N, O, P, and S are opposite.

Furthermore, the effects of concentration and temperature can be introduced into Cu nanotwin formation energy to explore their influences on the stability of Cu nanotwins. The part of nanotwin formation energy resulted from temperature (K) and alloying concentration (C) effects, $\Delta\gamma(K, C)$, can be calculated according to the following formula [48]:

$$\Delta\gamma(K,C)=\frac{\sum C_{T-x}(K)E_{se}}{2A}, \tag{7}$$

where C_{T-x} is the concentration of the alloying atom X in the n-th layer [49]:

$$C_{T-x}(K)=\frac{1}{1+\exp\left(\frac{E_{SF}}{KT}-\ln\left(\frac{c_0}{1-c_0}\right)\right)}, \tag{8}$$

where c_0 is the concentration of the alloying element. The calculated $\Delta\gamma(K, C)$ for metal elements (i.e., Li, Sn) and nonmetal ones (i.e., C and O) in four nanotwin configurations (4lnt, 6lnt, 8lnt, 10lnt) are displayed in Figures 9 and 10, respectively, to explore the joint effects of temperature (K) and alloying concentration. While the range of $\Delta\gamma(K, C)$ for Li and Sn is from −10 to 30 mJ/m^2 in Figure 9, that for C and O is from −30 to 0 mJ/m^2 in Figure 10. The values of $\Delta\gamma(K, C)$ for Li and Sn are bigger than those for C and O, which is in accordance with the results in Figure 8.

As shown in Figure 9, the change trends of $\Delta\gamma(K, C)$ for metal elements (i.e., Li and Sn) are similar under the joint influence of temperature and concentration. In 4lnt supercell, $\Delta\gamma(K, C)$ is lowest with the blue color for Li and Sn, and then $\Delta\gamma(K, C)$ increases in 6lnt, indicating that the configurations of different nanotwins can also affect $\Delta\gamma(K, C)$. Especially for 8lnt and 10lnt, Li and Sn can drastically result in a big value of $\Delta\gamma(K, C)$ at relatively high temperature and alloying concentration.

However, the values of $\Delta\gamma(K, C)$ are all negative for nonmetal elements (i.e., C and O) in Figure 10, which is directly associated with the strong bonding between Cu and each of them as stated in the above section. For nonmetal elements, C and O can strongly increase $\Delta\gamma(K, C)$ at relatively high temperature and low alloying concentration, which is different from the results of metal elements in Figure 9.

3.4 Generalized stacking fault energy and the nanotwin ductility

GSFE is an important energy value carried in the atomic-

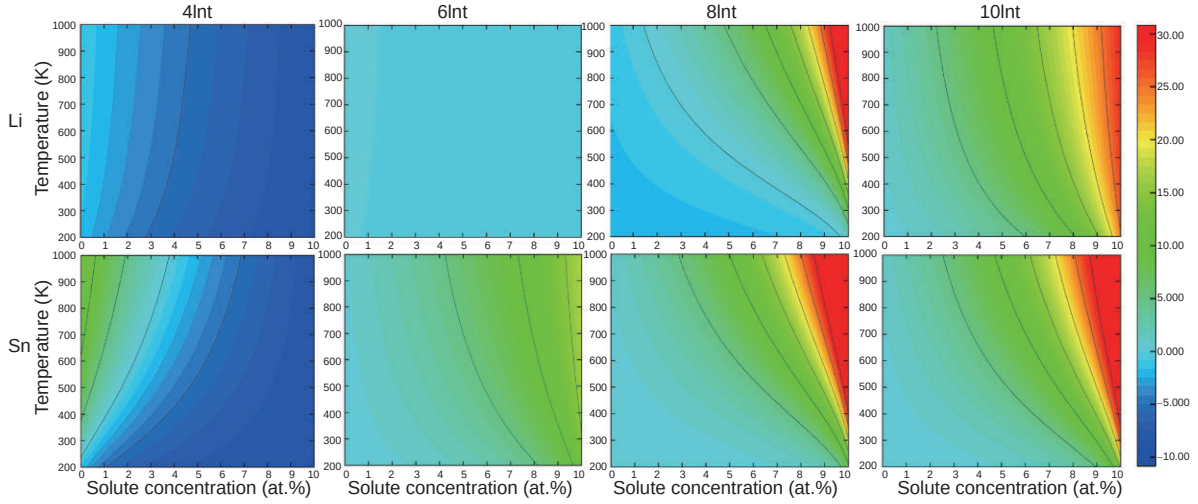

Figure 9 (Color online) Calculated $\Delta\gamma(K, C)$ (mJ/m^2) as a function of solute concentrations (c_0) and temperatures for Li and Sn elements in 4lnt, 6lnt, 8lnt and 10lnt nanotwin structures.

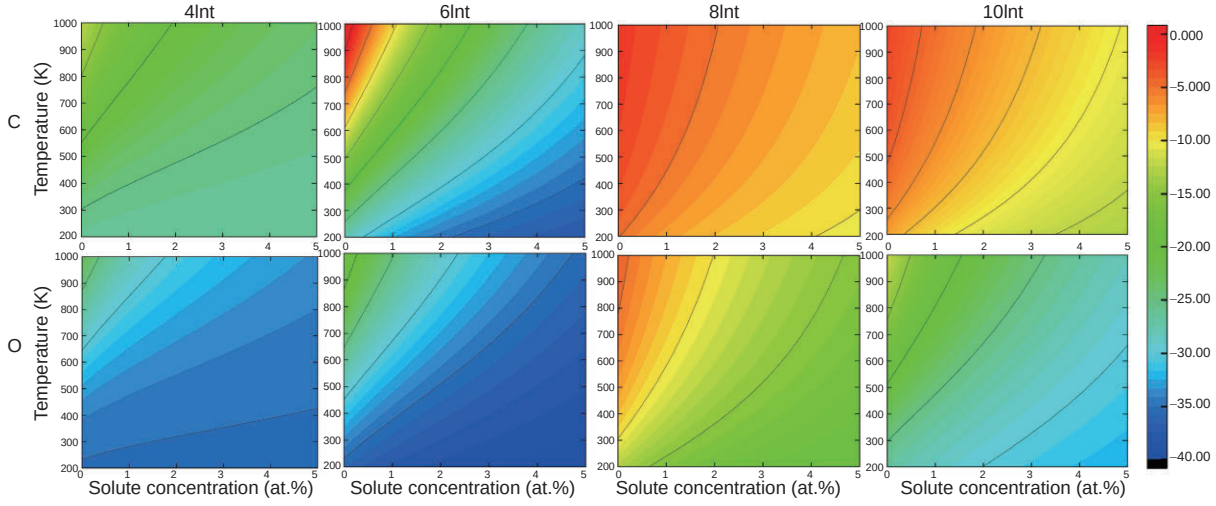

Figure 10 (Color online) Calculated $\Delta\gamma(K, C)$ (mJ/m^2) as a function of solute concentrations (c_0) and temperatures for C and O elements in 4lnt, 6lnt, 8lnt and 10lnt nanotwin structures.

level shear process on the slip plane. It can be determined using first-principles calculation to describe the macroscopic mechanical properties [37,38]. As stated in sect. 3.2, the bonds between Cu and the nonmetal elements are not the typical metal bonding and are much stronger; this will strongly hinder the shear process near the nonmetal elements. As a result, the slip plane will be away from the nonmetal elements, and the shear process will happen on the slip plane of pure Cu. Therefore, only substitutional metal atoms were considered when calculating the GSFE in this work.

The energies of the Cu nanotwins in this section were investigated by using the calculation model in Figure 2. Here, the nanotwin energy without the effects of temperature and concentration can be calculated as follows [47]:

$$\gamma = \frac{E_{X1} - E_{X0}}{A}, \tag{9}$$

where E_{X0} is the calculated energy of the FCC supercell in pure or doped Cu nanotwin (e.g., the supercell in Figure 2(a)), and E_{X1} is the energy of this system after introducing nanotwin (e.g., the supercells in Figures 2(b) and (c)). A is the area of the nanotwin plane in the supercell, denoted by the red lines in Figure 2. Since there is only one nanotwin plane in Figure 2, the denominator in eq. (9) is A, not $2A$. The nanotwin energies of NTB1 and NTB2 are denoted by γ_1 and γ_2, respectively, and the energy barrier from NTB1 to NTB2 is γ_{us}, as displayed in Table 2.

It can be found that $\gamma_1 > \gamma_2$ in Cu nanotwins with most substitutional alloying atoms (except Sn), and so Cu nanotwin is more stable when alloying atoms occupy the sites at the nanotwin boundary from an energetic viewpoint, indicating that Cu nanotwin has a tendency to accommodate substitutional alloying atoms. This is consistent with the above results of segregation energies in sect. 3.1.

The GSFE of substitution elements can be obtained by calculating the migration process of the nanotwin plane from NTB1 supercell to NTB2 supercell as shown in Figure 2. In Figure 11, the calculated results show that the energy sketch in doped Cu nanotwins display the similar change trend to that in pure Cu nanotwin. The calculated GSFEs are the values of $(\gamma_{us} - \gamma_1)$ or $(\gamma_{us} - \gamma_2)$ listed in Table 2, depending on the diffusion direction in Figure 2. With a low value of GSFE, it is easy for the atomic-level shear process on the slip plane to occur, and vice versa. Judged by the results listed in Table 2, Li, Mg and Sn can promote the atomic-level shear process on the slip plane, while Al will hinder this process. The effect of Zn is not obvious, since its values in Table 2 is close to that of the pure Cu nanotwin.

The values of $(\gamma_{us} - \gamma_1)$ or $(\gamma_{us} - \gamma_2)$ can also be used to identify the degree of difficulty for nanotwin diffusion towards and away from substitutional alloying atoms, respectively. With the bigger value of $(\gamma_{us} - \gamma_1)$ and $(\gamma_{us} - \gamma_2)$ than that of pure Cu nanotwin in Table 2, Al substitution can increase the energy barrier for nanotwin diffusion across it and thus inhibit the migration of the nanotwin boundary. Inversely, the effects of Li, Mg and Sn substitutions are opposite and can promote the nanotwin migration more than a pure Cu nanotwin. The effect of Zn is not evident, since the values of $(\gamma_{us} - \gamma_1)$ and $(\gamma_{us} - \gamma_2)$ in Zn doped Cu nanotwin are very close to those in pure Cu nanotwin.

Furthermore, the calculated γ_{us} can be used to investigate the effects of alloying elements on the ductility of Cu alloys in the framework of Rice-criterion ductility analysis [52-54], which describes the competition between the formation of dislocations from the crack tip and crack cleavage [55]. The ductility parameter, λ, can be calculated as follows:

$$\lambda \approx \frac{0.3\gamma_s}{\gamma_{us}} \tag{10}$$

in which γ_s denotes the surface energy. According to Rice-criterion ductility analysis, if λ>1, the alloys will be ductile under opening mode loading because of the smaller dislocation nucleation energy compared with the crack cleavage energy barrier [55].

The calculation results are displayed in Table 3, and it can

Table 2 The nanotwin energy and GSFE calculated by the CNEB method (mJ/m^2). The bold type represents the corresponding results from the references

	Cu	Li	Mg	Al	Zn	Sn
γ_1	16.9 (**16**) [50]	16.5	10.1	21.4	6.3	–26.7
γ_{us}	154.2 (**140**) [51]	118.8	93.0	132.5	139.3	12.4
γ_2	16.6	0.6	–0.0	–0.5	4.3	–29.6
γ_{us}–γ_1	137.3	102.3	82.9	153.9	133	39.1
γ_{us}–γ_2	137.6	118.2	93.0	133.0	135.0	42.0

Table 3 Calculated relative surface energy (γ_s) and Rice-criterion ductility (λ)

	Cu	Li	Mg	Al	Zn	Sn
γ_s (mJ/m^2)	2791.47	2696.35	2204.94	2751.16	2287.00	763.63
λ	5.43	6.81	7.11	6.23	4.93	18.47

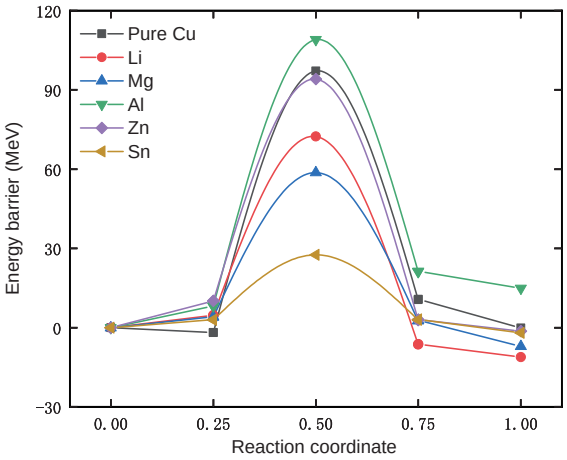

Figure 11 (Color online) Energy profile for pure and doped Cu supercells in the migration process of the nanotwin plane from NTB1 supercell to NTB2 supercell in Figure 2. The energies of the initial states are set to be zero for comparison.

be found that $1<\lambda(\mathrm{Zn})<\lambda(\mathrm{Cu})<\lambda(\mathrm{Al})<\lambda(\mathrm{Li})<\lambda(\mathrm{Mg})<\lambda(\mathrm{Sn})$. The λ value of Cu-Zn alloy is the smallest, which means that Zn addition can reduce the energy of dislocation nucleation and promote dislocation slip. Therefore, the toughness of Cu-Zn alloy is higher and prone to ductile fracture. Similarly, the larger the λ value of the metal element (i.e., Li, Mg, Al, Zn, and Sn) the smaller the energy barrier for overcoming dislocation slip and a larger value of λ can improve the forming ability of the alloy.

Our theoretical work at the atomic scale excludes any effects of the concentration of alloying element or other related effects. In particular, when the concentration increases, the effects of the interactions between the alloying elements become more important, which need serious considerations and will be addressed in our future studies.

4 Conclusion

In this work, we used first-principles calculations to study the alloying effects on the segregation energies in Cu nanotwins, their mechanical and chemical components, the nanotwin formation energies with temperature and concentration considerations and the generalized stacking fault energy in doped Cu nanotwins. The main conclusions are summarized as follows:

First, Cu nanotwin attracts alloying elements: substitutional metal or interstitial nonmetal elements. The segregation energy of the interstitial atom is mostly negative and lower than that of the substitutional atom.

Secondly, the segregation energy of the alloying element was decomposed into the mechanical and chemical components. The strong bond between Cu and the nonmetal element results in the negative value of the chemical contribution.

Thirdly, while metal elements (i.e., Li and Sn) can drastically result in a big value of $\Delta\gamma(K, C)$ at relatively high temperature and alloying concentration, nonmetal elements (i.e., C and O) can strongly increase it at relatively high temperature and low alloying concentration.

Finally, the bonds between Cu and the nonmetal elements can strongly hinder the shear process near the nonmetal elements; thus, only the substitutional metal atoms were considered when calculating the GSFE. Al can inhibit the migration of Cu nanotwin boundary, and the effects of Li, Mg and Sn are opposite.

This work was supported by the National Natural Science Foundation of China (Grant Nos. 11832019, 51601212, 11472313, and 11572355).

1 C. M. Grigorian, and T. J. Rupert, Acta Mater. **179**, 172 (2019).
2 M. A. Meyers, A. Mishra, and D. J. Benson, Prog. Mater. Sci. **51**, 427 (2006).
3 K. S. Kumar, H. Van Swygenhoven, and S. Suresh, Acta Mater. **51**, 5743 (2003).
4 H. V. Atkinson, Acta Metall. **36**, 469 (1988).
5 S. Simões, R. Calinas, M. T. Vieira, M. F. Vieira, and P. J. Ferreira, Nanotechnology **21**, 145701 (2010).
6 O. Renk, V. Maier-Kiener, I. Issa, J. H. Li, D. Kiener, and R. Pippan, Acta Mater. **165**, 409 (2019).
7 H. Gleiter, Prog. Mater. Sci. **33**, 223 (1989).
8 X. Huang, N. Hansen, and N. Tsuji, Science **312**, 249 (2006).
9 T. J. Rupert, J. R. Trelewicz, and C. A. Schuh, J. Mater. Res. **27**, 1285 (2012).
10 J. Hu, Y. N. Shi, X. Sauvage, G. Sha, and K. Lu, Science **355**, 1292 (2017).
11 Z. Han, L. Lu, and K. Lu, Tribol Lett **21**, 45 (2006).
12 K. Lu, L. Lu, and S. Suresh, Science **324**, 349 (2009).
13 W. Zhao, N. Tao, J. Guo, Q. Lu, and K. Lu, Scripta Mater. **53**, 745 (2005).
14 Y. H. Zhao, X. Z. Liao, Y. T. Zhu, Z. Horita, and T. G. Langdon, Mater. Sci. Eng.-A **410-411**, 188 (2005).
15 Y. H. Zhao, Y. T. Zhu, X. Z. Liao, Z. Horita, and T. G. Langdon, Appl. Phys. Lett. **89**, 121906 (2006).
16 Y. H. Zhao, X. Z. Liao, Z. Horita, T. G. Langdon, and Y. T. Zhu, Mater. Sci. Eng.-A **493**, 123 (2008).
17 Y. H. Zhao, J. F. Bingert, Y. T. Zhu, X. Z. Liao, Z. V. Ruslan, Z. Horita, T. G. Langdon, and Y. Z. Zhou, Appl. Phys. Lett. **92**, 081903 (2008).
18 V. Randle, Acta Mater. **47**, 4187 (1999).
19 E. El-Danaf, S. R. Kalidindi, and R. D. Doherty, Metall Mat Trans A **30**, 1223 (1999).
20 A. Rohatgi, and K. S. Vecchio, Mater. Sci. Eng.-A **328**, 256 (2002).
21 Y. H. Zhao, Y. T. Zhu, X. Z. Liao, Z. Horita, and T. G. Langdon, Mater. Sci. Eng.-A **463**, 22 (2007).
22 Z. Guo, A. P. Miodownik, N. Saunders, and J. P. Schillé, Scripta Mater. **54**, 2175 (2006).
23 T. H. Lee, E. Shin, C. S. Oh, H. Y. Ha, and S. J. Kim, Acta Mater. **58**, 3173 (2010).
24 Y. Zhang, N. R. Tao, and K. Lu, Acta Mater. **56**, 2429 (2008).
25 J. F. Nie, Y. M. Zhu, J. Z. Liu, and X. Y. Fang, Science **340**, 957 (2013).
26 Y. Chen, Y. K. Cheng, R. B. Zhu, F. F. Wang, H. T. Cheng, Z. H. Liu, C. X. Fan, Y. X. Xue, Z. C. Yu, J. K. Zhu, X. Y. Hu, and Q. H. Gong, Sci. China-Phys. Mech. Astron. **62**, 044201 (2019).
27 L. Huang, M. Z. Zhong, H. X. Deng, B. Li, Z. M. Wei, J. B. Li, and S.

H. Wei, Sci. China-Phys. Mech. Astron. **62**, 037311 (2019).
28 H. Y. Lv, G. H. Zhong, M. Chen, C. L. Yang, X. J. Chen, and H. Q. Lin, Sci. China-Phys. Mech. Astron. **62**, 957412 (2019).
29 Z. M. Shi, X. J. Sun, Y. P. Jia, X. K. Liu, S. L. Zhang, Z. B. Qi, and D. B. Li, Sci. China-Phys. Mech. Astron. **62**, 127311 (2019).
30 C. Zhang, Y. Yang, and P. Zhang, Sci. China-Phys. Mech. Astron. **62**, 107002 (2019).
31 A. Kumar, J. Wang, and C. N. Tomé, Acta Mater. **85**, 144 (2015).
32 X. Zhou, and J. Song, Acta Mater. **148**, 9 (2018).
33 T. Fan, L. Wei, B. Tang, L. Peng, and W. Ding, Philos. Mag. **94**, 1578 (2014).
34 G. H. Xiao, N. R. Tao, and K. Lu, Scripta Mater. **65**, 119 (2011).
35 V. Vítek, Philos. Mag. **18**, 773 (1968).
36 Y. T. Zhu, X. Z. Liao, and X. L. Wu, Prog. Mater. Sci. **57**, 1 (2012).
37 G. Lu, N. Kioussis, V. V. Bulatov, and E. Kaxiras, Phys. Rev. B **62**, 3099 (2005), arXiv: cond-mat/9903440.
38 M. Muzyk, Z. Pakiela, and K. J. Kurzydlowski, Scripta Mater. **66**, 219 (2012).
39 K. F. Garrity, J. W. Bennett, K. M. Rabe, and D. Vanderbilt, Comput. Mater. Sci. **81**, 446 (2014).
40 G. Kresse, and J. Furthmüller, Phys. Rev. B **54**, 11169 (1996).
41 P. Hohenberg, and W. Kohn, Phys. Rev. **136**, B864 (1964).
42 W. Kohn, and L. J. Sham, Phys. Rev. **140**, A1133 (1965).
43 P. E. Blöchl, Phys. Rev. B **50**, 17953 (1994).
44 J. P. Perdew, J. A. Chevary, S. H. Vosko, K. A. Jackson, M. R. Pederson, D. J. Singh, and C. Fiolhais, Phys. Rev. B **46**, 6671 (1992).
45 M. Yamaguchi, M. Shiga, and H. Kaburaki, Science **307**, 393 (2005).
46 S. Zhang, O. Y. Kontsevoi, A. J. Freeman, and G. B. Olson, Phys. Rev. B **84**, 134104 (2011).
47 J. Han, X. M. Su, Z. H. Jin, and Y. T. Zhu, Scripta Mater. **64**, 693 (2011).
48 Q. Q. Shao, L. H. Liu, T. W. Fan, D. W. Yuan, and J. H. Chen, J. Alloys Compd. **726**, 601 (2017).
49 T. W. Fan, Z. P. Wang, J. J. Lin, D. C. Chen, Q. H. Fang, T. Hu, B. H. Nie, K. Wang, H. W. Hu, H. B. Sun, H. Y. He, L. Ma, and P. Y. Tang, J. Alloys Compd. **783**, 765 (2019).
50 S. Ogata, J. Li, and S. Yip, Science **298**, 807 (2002).
51 J. Bezares, S. Jiao, Y. Liu, D. Bufford, L. Lu, X. Zhang, Y. Kulkarni, and R. J. Asaro, Acta Mater. **60**, 4623 (2012).
52 E. B. Tadmor, and S. Hai, J. Mech. Phys. Solids **51**, 765 (2003).
53 E. B. Tadmor, and N. Bernstein, J. Mech. Phys. Solids **52**, 2507 (2004).
54 R. J. Asaro, and S. Suresh, Acta Mater. **53**, 3369 (2005).
55 M. B. Kivy, and M. A. Zaeem, Scripta Mater. **139**, 83 (2017).